Magic Numbers for the Photoelectron Anisotropy in Li-Doped Dimethyl Ether Clusters

Published as part of The Journal of Physical Chemistry virtual special issue "Hanna Reisler Festschrift".

Jonathan V. Barnes, Bruce L. Yoder, and Ruth Signorell*

ETH Zürich, Laboratory of Physical Chemistry, Vladimir-Prelog-Weg 2, CH-8093 Zürich, Switzerland

S *Supporting Information*

ABSTRACT: Photoelectron velocity map imaging of Li-$(CH_3OCH_3)_n$ clusters ($1 \leq n \leq 175$) is used to search for magic numbers related to the photoelectron anisotropy. Comparison with density functional calculations reveals magic numbers at $n = 4$, 5, and 6, resulting from the symmetric charge distribution with high s-character of the highest occupied molecular orbital. Since each of these three cluster sizes correspond to the completion of a first coordination shell, they can be considered as "isomeric motifs of the first coordination shell". Differences in the photoelectron anisotropy, the vertical ionization energies and the enthalpies of vaporization between $Li(CH_3OCH_3)_n$ and $Na(CH_3OCH_3)_n$ can be rationalized in terms of differences in their solvation shells, atomic ionization energies, polarizabilities, metal−oxygen bonds, ligand−ligand interactions and by cooperative effects.
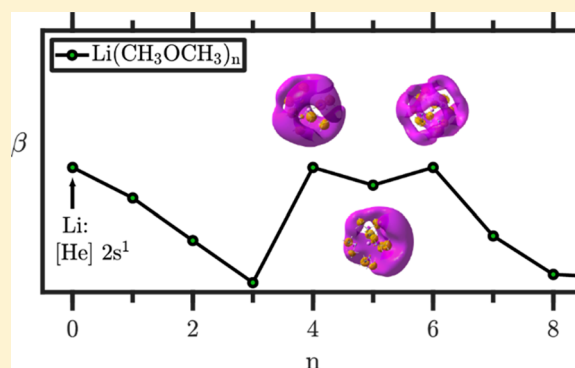
1. INTRODUCTION

Magic numbers play a central role in cluster science (see, e.g., refs 1−12). Usually, these magic numbers are related to the high stability of clusters of certain sizes. By contrast, reports on magic numbers related to photoelectron anisotropy are comparatively sparse.[10,11,13,14] This is because measurements of photoelectron angular distributions (PADs) of clusters are not so common and the modeling of cluster PADs is demanding.[5,10,11,13−29] Typically, a prerequisite for the observation of magic numbers in the photoelectron anisotropy is a high cluster symmetry that results in orbitals with high fractional s-character.[10,13,14,24]

In our recent studies,[10,24] we reported the first observation of magic numbers in the photoelectron anisotropy of solvated electrons in Na-doped clusters of dimethyl ether, ammonia, methanol, and water. The studies have revealed that in clusters of high symmetry the solvated electron can delocalize over extended regions, forming symmetric charge distributions of high s-character. However, they have also shown that the direct experimental observation of magic clusters can be hindered by several factors. An important factor is the lack of size selection for the neutral clusters under investigation. This results in PADs that are averages of several cluster sizes, making the detection of magic numbers more difficult. Furthermore, many structural isomers with similar energies can occur in these weakly bound systems, again making the observation of magic numbers less likely compared with systems that exhibit fewer structural isomers. Our calculations showed that in particular the strong hydrogen bonds in the Na-doped methanol and

water clusters result in a large number of isomers. In addition, these systems tend to prefer nonsymmetric structures with the Na and the electron pushed to one side of the cluster to minimize the perturbation of the hydrogen bond network. Given these facts, it is thus not so surprising that the clearest experimental result for a magic number cluster was found for Na-doped dimethyl ether clusters, namely, for the hexamer $Na(CH_3OCH_3)_6$, which has near T_h symmetry with an octahedral coordination of Na by the CH_3OCH_3 molecules. The lack of strong hydrogen bonding in these clusters strongly reduced the number of isomers, and in addition the hexamer was also found to be a particularly stable structure; i.e., it is also a magic number cluster with respect to stability. High level quantum chemical calculations for $Na(CH_3OCH_3)_n$ and $Na(NH_3)_n$ clusters by Gunina and Krylov[11] are in agreement with our previous experimental results[10,24] and provide a detailed understanding of the underlying phenomena regarding the character of the electronic structure and the influence of structural fluctuations on the electronic properties.

The present study focuses on magic numbers in the photoelectron anisotropy of Li-doped dimethyl ether clusters $(Li(CH_3OCH_3)_n)$. Many aspects of Li-doped molecular clusters have been investigated in detail (see refs 9 and 30−36 and references therein) but to the best of our knowledge no angle-resolved photoelectron spectra have

been reported so far. Li is smaller and less polarizable than Na, which, for example, lets one expect that the almost perfect T_h symmetry with octahedral coordination of the Na core in $Na(CH_3OCH_3)_6$ might be distorted in the Li-doped hexamer so that the magic number cluster might shift to another cluster size than the hexamer. The goal of the present work is to unravel how the substitution of the alkali metal in dimethyl ether clusters influences the energetics, structure, and magic numbers by a combination of experimental data and density functional theory (DFT) calculations.

2. EXPERIMENT

The experimental setup, the measurement procedures, and the data analysis are essentially identical to those used in our previous investigations of $Na(CH_3OCH_3)_n$ clusters.[10,24] For convenience, we repeat here the main aspects as provided in the experimental part of West et al.[10] The experimental setup has been previously described in detail.[21−24,37−39]

All measurements were performed in a velocity map imaging (VMI)[40,41] photoelectron spectrometer, which can also function as a time-of-flight mass spectrometer. $(CH_3OCH_3)_n$ solvent clusters were generated by pulsed supersonic expansion of a He/CH_3OCH_3 gas mixture into vacuum. The solvent cluster size was varied from one molecule up to a maximum of approximately 175 molecules per cluster by varying the expansion conditions (backing pressure, gas composition, pressure, nozzle temperature) and oven temperature. The solvent clusters were doped with a single Li atom in a Li oven, which was heated to a temperature of 650 K. The resulting $Li(CH_3OCH_3)_n$ clusters were ionized with a 266 nm pulse from an Nd:YAG laser (photon energy of 4.66 eV), which exclusively ionized the unpaired (solvated) electron. The cluster size distributions were determined by mass spectrometry, which through the cluster mass provides information on the number of solvent molecules n per cluster.[21,24,37] For small clusters ($n \leq 4$) we use the actual number of molecules n to assign a cluster size, while the cluster size distributions for large clusters are characterized by the average cluster size $\langle n \rangle$ (and sometimes in addition by the maximum cluster size n_{max}). As exemplified by the relatively high intensity of the Na-$(CH_3OCH_3)_6$ mass peak in Figure 2f of West et al.,[10] relative intensities of clusters of different sizes in mass spectra can provide information on cluster stability (magic numbers related to cluster stability).

Information on cluster-size-dependent photoelectron angular distributions (PAD) and photoelectron kinetic energies are retrieved from the velocity map photoelectron images after reconstruction with MEVIR[42] (note that reconstruction with pBASEX[43] provides very similar results). Experimental electron binding energy (eBE) spectra are determined from the difference between the photon energy (4.66 eV) and the recorded photoelectron kinetic energy spectrum. The experimental ionization energies IE_{max} for different cluster sizes are determined at the maxima of the photoelectron bands using Gaussian/Lorentzian fits. It is generally assumed that the IE_{max} lie close to the values for the calculated vertical ionization energies IE_{vert} (section 3). We characterize the PAD by the anisotropy parameter β,[44]

$$\frac{d\sigma}{d\Omega} = \frac{\sigma_{tot}}{4\pi}\left[1 + \frac{\beta}{2}(3\cos^2\theta - 1)\right] \qquad (1)$$

$\frac{d\sigma}{d\Omega}$ and σ_{tot} are the differential and the total photoionization cross section, respectively, and θ is the angle between the photoelectron velocity vector and the polarization axis of the incident light. The indicated experimental cluster-size-dependent β-parameters are determined from an average over 11 pixels, including 5 pixels on each side of the peak maximum in the eBE spectra. As in our previous study,[10] we estimate the relative uncertainty of IE_{max} and β as a function of cluster size to be on the order of 5% in both cases. The absolute uncertainties in IE_{max} and β are on the order of ±0.1 eV and ±0.1, respectively.

3. DFT CALCULATIONS

The experimental results are compared with various quantities (β-parameters, vertical ionization energies IE_{vert}, enthalpies of vaporization H_{vap}, and dipole moments) obtained from calculations with the Gaussian program package[45] using the dispersion corrected ωB97XD density functional with a 6-31+G* basis set. The calculations are analogous to those for $Na(CH_3OCH_3)_n$ clusters,[10,24] the most important aspects of which we repeat here for convenience. H_{vap} is calculated for the neutral clusters as the total dissociation energy divided by the number of solvent monomer units. It is used here to compare cluster stabilities for different cluster sizes. The calculated total dipole moment of the different neutral clusters is used as a simple but very sensitive measure of the displacement of the charge distribution. IE_{vert} are compared with the experimental IE_{max}. IE_{vert} are obtained by subtracting the energy of the neutral cluster from the energy of the ionic cluster with the same geometry. The calculated β-parameters are determined as previously explained in detail[10] and in the Supporting Information of West et al.[24] Briefly, the highest occupied molecular orbital (HOMO) is expanded in terms of atomic natural orbitals (ANOs).[46] In order to account for the polarization of the HOMO upon solvation, we use an expanded valence shell including 2p functions on Li for the ANO analysis (NBO program version 3.1). The normalized angular momentum (l) character c_l^2 of the HOMO is calculated as the sum over ANO contributions of the same l. The β-parameters are then obtained from[17]

$$\beta = \sum_l c_l^2 \beta_l \qquad (2)$$

with β_l determined from the Cooper−Zare formula,[44]

$$\beta_l = \frac{l(l-1)(1-R)^2 + (l+1)(l+2)R^2 - 6l(l+1)(1-R)R}{(2l+1)[l(1-R)^2 + (l+1)R^2]} \qquad (3)$$

R is the relative radial dipole matrix element of the $(l+1)$ partial wave. We neglect the phase shift between outgoing partial waves. Furthermore, we provide here the results for $R = 0.5$ and for radial matrix elements that vanish at all centers except at the Li atom. We have previously shown for Na-doped clusters that the size dependence of β (not the actual values) is almost independent of the choice of the parameters (i.e., other limiting cases for R and for radial matrix elements for all atomic centers).[24] In Li-doped and Na-doped clusters, the unpaired electron largely retains the character of the Li and Na valence electron, respectively. The above-mentioned robustness with respect to the model parameters derives from precisely this

special property of the unpaired electron in the clusters, and enables us to derive meaningful results from the simple approach in eqs 2 and 3. Note that trends in the size-dependence of calculated and experimental β-parameters can be compared, even though their actual values cannot.

4. RESULTS FOR Li(CH$_3$OCH$_3$)$_n$ CLUSTERS

As an example, Figure 1 shows a photoelectron image for small Li(CH$_3$OCH$_3$)$_n$ clusters with $n \leq 4$ together with the
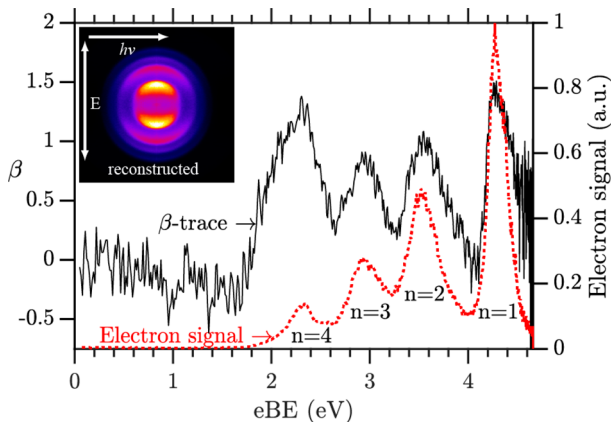

Figure 1. Inset: reconstructed photoelectron images of Li-(CH$_3$OCH$_3$)$_n$ clusters with $n = 1-4$ solvent molecules. Full black line: β-trace as a function of the electron binding energy (eBE). Dotted red line: Photoelectron spectrum as a function of eBE.

corresponding energy-dependent β-trace (full black line) and the photoelectron spectrum (dotted red line) as a function of the eBE. For these small clusters, the different rings in the image, the different bands in the energy-dependent β-trace, and the resolved bands in the photoelectron spectrum can be

assigned to specific cluster sizes. The image and the β-trace show that the PAD remains clearly anisotropic (large values of the β-parameters at the band maxima), while the photoelectron spectrum reveals a very strong decrease in IE$_{max}$ by around 2 eV with increasing cluster size from $n = 1$ to $n = 4$. For Li-doped clusters, truly size-resolved data could only be obtained up to $n = 4$. As shown in Figure 2a, the photoelectron bands of larger clusters lie too close in energy to resolve specific cluster sizes. We thus assign an average cluster size $\langle n \rangle$ to these merged bands (see bands for $\langle n \rangle = 20$ and $\langle n \rangle = 63$ in Figure 2a). Parts b and c of Figure 2 show representative mass spectra for the cases $n = 1-4$ and $\langle n \rangle = 63$, respectively. The decrease in IE$_{max}$ with increasing cluster size is systematic but rather moderate beyond $n = 4$ (see Figures 3g and 4b and Table S1 in the Supporting Information). The evolution of the β-parameter with increasing cluster size is more complicated. Its value strongly decreases from $\beta = 1.4$ to $\beta = 0.8$ between $n = 1$ and $n = 3$, to peak again at $n = 4$ with a value of $\beta = 1.3$. Beyond $n = 4$ we lose cluster size resolved information. However, the fact that β stays fairly high up to $\langle n \rangle = 20$ (see Figures 3e and 4c and Table S1 in the Supporting Information) implies that *several* clusters with sizes larger than $n = 4$ must also have fairly high β-parameters. At first sight, this result appears rather surprising.

To better understand this behavior, we have performed DFT calculations to obtain structures and β-parameters for clusters with up to 20 molecules (see Figure 3 and Table S2 in the Supporting Information). The calculated β-parameter of 2 in Figure 3a and the isosurface of the HOMO in Figure 5a clearly reveal the tetramer Li(CH$_3$OCH$_3$)$_4$ as a magic cluster with respect to the photoelectron anisotropy consistent with the experiment (Figure 3e). This cluster has a highly symmetric structure with a tetrahedral coordination of the Li core by the ligands and a symmetric HOMO that is delocalized over an almost spherical shell around the cluster (Figure 5a). As a
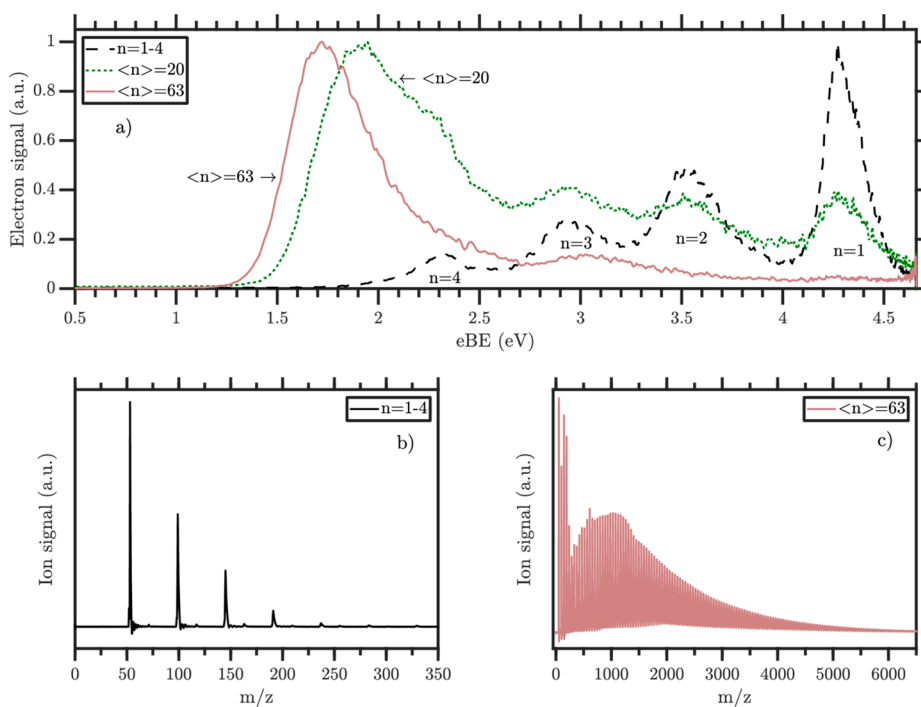

Figure 2. (a) Photoelectron spectra of Li(CH$_3$OCH$_3$)$_n$ clusters as a function of eBE. Dashed black line: $n = 1-4$. Dotted green line: $\langle n \rangle = 20$. Full red line: $\langle n \rangle = 63$. (b) Mass spectrum for $n = 1-4$. (c) Mass spectrum for $\langle n \rangle = 63$.
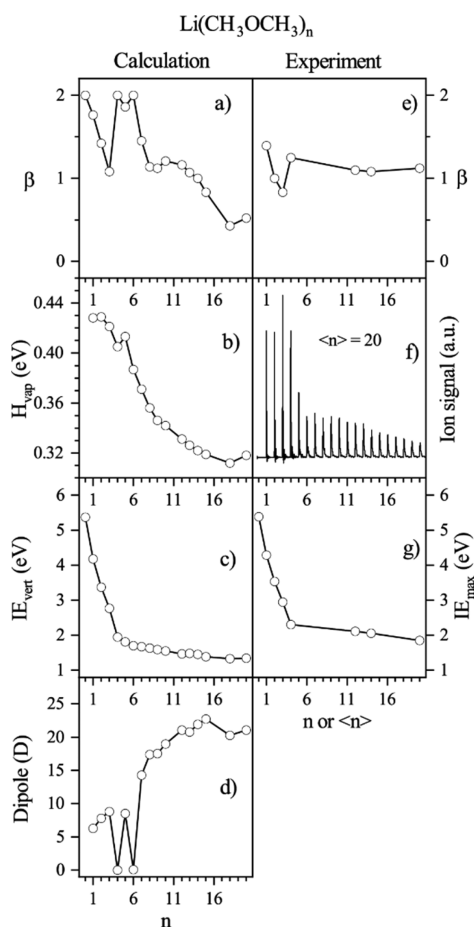
Figure 3. Properties of $Li(CH_3OCH_3)_n$ clusters as a function of the number of solvent molecules n: (a) calculated β-parameters, (b) calculated enthalpies of vaporization H_{vap}, (c) calculated vertical ionization energies IE_{vert}, (d) calculated dipole moments, (e) experimental β-parameters, (f) representative mass spectrum for $\langle n \rangle$ = 20, and (g) experimental ionization energies determined at the maximum of the photoelectron bands IE_{max}. For the calculations, the open circles connected by lines are the values for the energetically lowest isomers. For other isomers see Table S2 in the Supporting Information.

Figure 4. Comparison of $Li(CH_3OCH_3)_n$ (open circles) and $Na(CH_3OCH_3)_n$ (open triangles) cluster data. (a) Calculated enthalpies of vaporization H_{vap}. (b) Experimental ionization energies IE_{max}. (c) Experimental β-parameters.

result, this HOMO has a very high s-character (100% in the calculation), which explains the high β value. The high symmetry is also reflected in the very low dipole moment (Figure 3d). However, H_{vap} in Figure 3b shows that $Li(CH_3OCH_3)_4$ is not particularly stable compared with the neighboring clusters of different sizes; i.e., it is not a magic cluster with respect to the stability. This is consistent with the experimental mass spectra, in which the mass signal does not peak at $n = 4$ (see example in Figures 2c and 3f). In the case of sodium clusters we had observed a rather different behavior, with the Na-hexamer $Na(CH_3OCH_3)_6$ as a magic cluster with respect to both stability and anisotropy (see Figures 2b,f in West et al.[10]). This difference between Li and Na can be rationalized by the balance between the electronic stabilization afforded by the metal–oxygen "bonds" on one hand and the steric destabilization due to crowding of ligands on the other hand. In small Na-clusters the former dominates, while the latter gains importance in Li-clusters as a result of the much smaller atomic radius and hence shorter metal–oxygen bond (see further below and section 5). $Li(CH_3OCH_3)_4$ shows a highly symmetric coordination with an almost perfect LiO_4
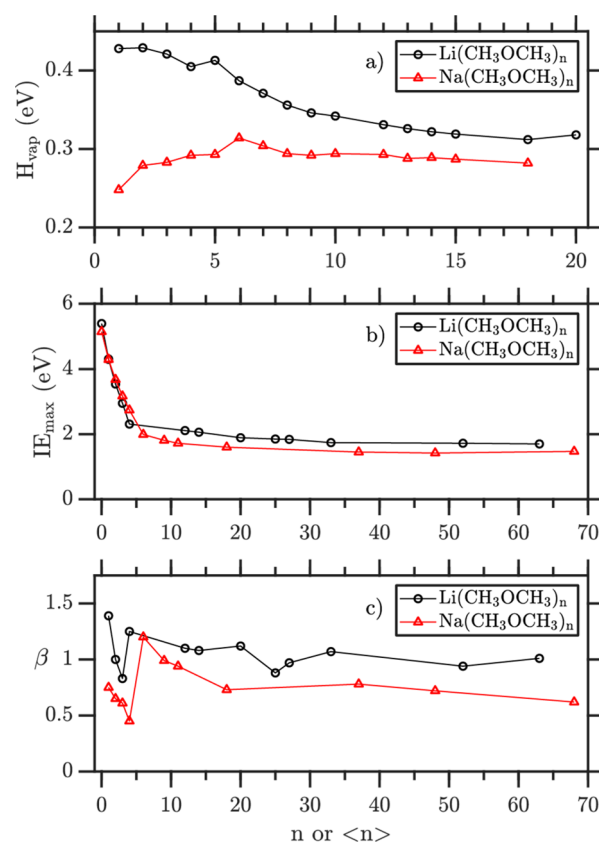
tetrahedron. The T_d symmetry is necessarily broken by the C_2 symmetry of the ligands resulting in a number of symmetry equivalent minima. At the ωB97XD/6-31+G* level the rotation angles around the C_3-axes of the LiO_4 tetrahedron are virtually all equal, resulting in a highly symmetric HOMO. As a result, the dipole moment almost vanishes and β reaches its maximum value of 2. At higher levels of electronic theory the symmetry of the equilibrium structure might be further broken, resulting in the localization of the unpaired electron at one side of the (approximate) tetrahedron, a correspondingly large dipole moment, and a reduction of the calculated β. Nevertheless, one would still expect to observe tetrahedral symmetry of the HOMO in the experiment. This is a consequence of the inverse Born–Oppenheimer (or sudden) character of the unpaired electron's wave function: very small nuclear displacements lead to a large change in the electronic wave function. Effectively, the unpaired electron will "see" a vibrationally averaged structure of the cluster. As long as the barrier between symmetry-equivalent minima remains small (as expected for small rotation angles around the C_3-axes of the LiO_4 tetrahedron), the vibrationally averaged structure will remain tetrahedral.

The next two larger cluster sizes, $Li(CH_3OCH_3)_5$ and $Li(CH_3OCH_3)_6$, have similarly high β-parameters as the tetramer (Figure 3a). This is rather surprising and different from the Na-case in West et al.[10] However, it supports our hypothesis that several clusters with sizes larger than $n = 4$ and high β-parameters are the reason for the experimentally observed trend of high β-values even up to $\langle n \rangle$ = 20 (Figure
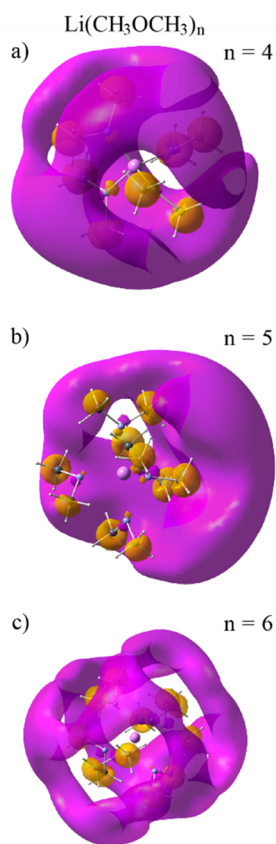
$Li(CH_3OCH_3)_n$

a) $n = 4$

b) $n = 5$

c) $n = 6$

Figure 5. Isosurfaces of the HOMO of the most stable isomers of (a) the $Li(CH_3OCH_3)_4$ cluster, (b) the $Li(CH_3OCH_3)_5$ cluster, and (c) the $Li(CH_3OCH_3)_6$ cluster. The calculated s-character of these HOMO are 100%, 95%, and 100%, respectively.

3e) because the contribution of the highly symmetric smaller cluster is high in the corresponding size distributions. The most stable pentamer has a trigonal-bipyramidal structure (Figure 5b) and the most stable hexamer has an octahedral structure (Figure 5c). To make space for the additional ligands in the expanded solvation shell, the Li−O distance increases. This weakening of the Li−O "bond" reduces H_{vap}. In the case of the pentamer, an axial distortion of the trigonal-bipyramidal structure counteracts this effect by reducing the unfavorable steric interaction between the ligands, so that overall H_{vap} even slightly increases compared with that for the tetramer (but still lies below that of the trimer). The crowding of ligands leads to an additional symmetry breaking in terms of the rotational angles of the three equatorial ligands around the Li−O "bonds". The ensuing localization of the unpaired electron on one side of the pyramid is reflected in the sizable dipole moment. The dominant s-character of the HOMO (95%) is much less affected by this localization with a correspondingly small reduction of the β value. In the hexamer cluster the further lengthening of the Li−O distance is the dominant effect, such that H_{vap} decreases significantly. The octahedral structure remains intact with a highly symmetric HOMO (100% s-character) and correspondingly vanishing dipole moment and maximal β value. All these clusters correspond to the completion of a first coordination shell, so that they can be considered as "isomeric motifs of the first coordination shell". This explains their similar values for β and IE_{vert} and their relatively high stability (high values of H_{vap}). Table S2 in the Supporting Information also lists data for a few isomers for

$n = 5$ and 6. Isomer a of the pentamer has a tetrahedral first ligand shell with one additional molecule added in the second shell. Its β value of 1.49 is significantly lower than that for the most stable isomer because of the lower symmetry. Similarly, isomers of the hexamer with a symmetric first ligand shell and additional molecules placed in the second shell also have low β values (isomer b with a first tetrahedral shell $\beta = 1.34$ and isomer a with a first bipyramidal ligand shell $\beta = 1.44$; see Table S2).

The PADs of even larger clusters are still anisotropic but with β values clearly below those of $n = 4$, 5, and 6 (Figure 3a). These clusters are less symmetric than the smaller ones with correspondingly lower β values and larger dipoles. The less symmetric structures, typically with the Li and its electron pushed to one side of the cluster (see Figure S1 in the Supporting Information for $n = 20$), allow the perturbation of the solvent molecules to be minimized, while keeping the unpaired electron close to the Li core and maximizing the strong favorable Li−O interactions in the first solvation shell. Table S2 in the Supporting Information lists the properties of some higher lying isomers. Among them are also highly symmetric isomers with high β values, such as isomer b for $n = 10$. For Li-clusters, H_{vap} decreases almost continuously with increasing cluster size (Figure 3b). For very large clusters it has to converge to the calculated bulk value of pure (without Li) dimethyl ether of about 0.23 eV (experimental bulk value around 0.29 eV).[47] For small clusters with one ligand shell (up to $n \sim 6$), H_{vap} is comparatively high because the strong Li−O bond dominates, partially counterbalanced by the steric interaction in the increasingly crowded ligand shell. With more ligands ($n \gtrsim 7$), the contribution of the Li−O bonds to H_{vap} is increasingly "diluted" by the much weaker ligand−ligand interaction in the outer shells and gradually converges to the bulk value. For IE_{vert}, pronounced changes are only observed until the completion of the first solvation shell at $n = 4$. The extension of the first shell in $n = 5$ and 6 retains a balance between the increase in the number of strong Li−O interactions and their weakening as a consequence of ligand crowding (bond lengthening). The further slow decrease of IE_{vert} beyond $n = 6$ can be attributed to increasing polarization effects (as the cluster's polarizability increases with its size).

5. COMPARISON OF $Li(CH_3OCH_3)_n$ AND $Na(CH_3OCH_3)_n$ CLUSTERS

Figure 4 provides a comparison of $Li(CH_3OCH_3)_n$ and $Na(CH_3OCH_3)_n$ cluster data. The behavior of H_{vap} for the Na-clusters differs pronouncedly from that of the Li-clusters (Figure 4a). Small Na-clusters have a lower H_{vap} that increases with cluster size, while small Li-clusters have a higher H_{vap} that decreases with cluster size. The maxima for H_{vap} are reached at the hexamer of Na and at the monomer for Li. The generally lower H_{vap} for small Na-clusters can likely be attributed to the weaker Na−O bond compared with the Li−O bond. As mentioned in section 4, the decrease of H_{vap} is consistent with a weakening (i.e., lengthening) of the Li−O bond because of the increased crowding of ligands in the first solvation shell. Given the much larger atomic radius of sodium, ligand crowding plays a less important (if any) role in small $Na(CH_3OCH_3)_n$ clusters. This would lead to the expectation of a roughly constant H_{vap} until the first solvation shell is complete at $n = 6$. The increase of H_{vap} observed instead points toward significant cooperative effects, possibly resulting in part from (weak) hydrogen bonding interactions between the

ligands. For larger clusters ($n > 6$), H_{vap} decreases again, but more slowly than for Li-clusters. This is in part a trivial consequence of the smaller difference between the Na−O bond strength and the ligand−ligand interaction (the "dilution" per ligand added is less in Na- than in Li-clusters). Another contributing factor is the larger polarizability of the 3s unpaired electron of Na as compared with the polarizability of the 2s electron of Li. The former more easily deforms to adapt to its position on the cluster surface.

In contrast to the trends in H_{vap}, the trends in IE_{max} are qualitatively identical for Na- and Li-clusters (Figure 4b). Strong decreases are only observed before the closure of the first solvation shells (at $n = 4$ for Li and $n = 6$ for Na), while for larger clusters the values of IE_{max} drop only very slowly as a result of the increasing overall polarizability of the cluster. For larger Li-clusters, the absolute values of IE_{max} observed experimentally lie systematically above those of the Na-clusters by about 0.3 eV. This difference approximately equals the difference between the ionization energies for atomic Na and Li (5.14 eV[48] and 5.39 eV,[49] respectively). The unpaired (surface-solvated) electron in the cluster apparently still feels the core it belonged to. This is consistent with the results of our DFT calculations. As mentioned above, the most stable larger clusters tend to have the metal core and the electron located at one side of the cluster close to the surface. The electron is thus still close to the respective metal core, which might explain the conservation of the shift between cluster and atomic metal.

Finally, Figure 4c compares the β-parameters for the two cases. The occurrence of magic clusters related to the anisotropy at $n = 6$ for Na-clusters and at $n = 4$, 5, and 6 for Li-clusters was already discussed in West et al.[10] and in section 4. Here, we additionally point out the general downshift of β of Na-clusters compared with results for Li-clusters observed experimentally for essentially all cluster sizes. This phenomenon is reproduced at least qualitatively by the DFT calculations. A lowering of β results from the polarization of the HOMO upon solvation, which gives rise to higher angular momentum components l (essentially $l = 1$) of the HOMO. A more polarizable atomic orbital is more easily distorted (polarized), i.e., more easily acquires higher l components upon solvation of the atom. The lower β values of the Na-clusters can thus be explained by the higher polarizability of the 3s electron compared with that of the 2s electron of Li.

6. SUMMARY

This paper compares properties of neutral $Li(CH_3OCH_3)_n$ and $Na(CH_3OCH_3)_n$ clusters with a focus on magic numbers related to the photoelectron anisotropies from the highest occupied molecular orbital, i.e., the solvated electron that can delocalize over extended cluster regions. In Li-doped clusters, magic numbers are observed at $n = 4$, 5, and 6 as a result of the completion of the first solvation shell. Such "isomeric motifs of the first coordination shell" were not observed for Na-doped clusters, which showed a distinct magic cluster at $n = 6$.[10] The difference between the two alkali metals seems to arise from a balance between the electronic stabilization by the metal−oxygen bonds and the steric destabilization due to crowding of ligands. The general lowering of the β-parameters to around 0.25 for Na-clusters compared with those for Li-clusters for clusters with up to $\langle n \rangle \approx 70$ can be explained by the higher polarizability of the 3s compared with that of the 2s electron. Similarly, a general lowering of the ionization energy by

approximately 0.3 eV of Na-clusters compared with results for Li-clusters is observed in the same cluster size range. It roughly matches the difference of the ionization energies of the two bare metals, which seems to be conserved in the molecular clusters. Both alkali metal clusters show a very pronounced decrease of the ionization energy by about 2 eV for small clusters before the closure of the first solvation shell. DFT calculations reveal a distinct difference between the behavior of the enthalpies of vaporization for the two metal clusters as a function of the cluster size, which can be rationalized by differences in the metal−oxygen bonds and the ligand−ligand interactions, in the polarizabilities of the 3s and 2s electrons, in the crowding of ligands, and by cooperative effects. Such cluster studies might also contribute to a better understanding of the properties of the solvated electron in the condensed phase.[9,50−61]

■ ASSOCIATED CONTENT

S Supporting Information

The Supporting Information is available free of charge on the ACS Publications website at DOI: 10.1021/acs.jpca.8b12262.

Table of experimental results of IE_{max} and β for various neutral cluster sizes, a table summarizing DFT calculation results for various cluster sizes ($1 \leq n \leq 20$), and a figure showing the isosurface of the HOMO of the most stable isomer for the $Li(CH_3OCH_3)_{20}$ cluster (PDF)

■ AUTHOR INFORMATION

Corresponding Author

*E-mail: rsignorell@ethz.ch.

ORCID ⓘ

Ruth Signorell: 0000-0003-1111-9261

Notes

The authors declare no competing financial interest.

■ REFERENCES

(1) Vafayi, K.; Esfarjani, K. Abundance of Nanoclusters in a Molecular Beam: The Magic Numbers for Lennard-Jones Potential. *J. Cluster Sci.* 2015, 26, 473−490.

(2) Coolbaugh, M. T.; Garvey, J. F. Magic Numbers in Molecular Clusters - a Probe for Chemical-Reactivity. *Chem. Soc. Rev.* 1992, 21, 163−169.

(3) Alonso, J. A. *Structure and Properties of Atomic Nanoclusters*; Imperial College Press: London, 2005.

(4) Chang, H. C.; Wu, C. C.; Kuo, J. L. Recent Advances in Understanding the Structures of Medium-Sized Protonated Water Clusters. *Int. Rev. Phys. Chem.* 2005, 24, 553−578.

(5) Young, R. M.; Neumark, D. M. Dynamics of Solvated Electrons in Clusters. *Chem. Rev.* 2012, 112, 5553−5577.

(6) Hammer, N. I.; Shin, J. W.; Headrick, J. M.; Diken, E. G.; Roscioli, J. R.; Weddle, G. H.; Johnson, M. A. How Do Small Water Clusters Bind an Excess Electron? *Science* 2004, *306*, 675−679.

(7) Turi, L.; Rossky, P. J. Theoretical Studies of Spectroscopy and Dynamics of Hydrated Electrons. *Chem. Rev.* 2012, *112*, 5641−5674.

(8) Zeuch, T.; Buck, U. Sodium Doped Hydrogen Bonded Clusters: Solvated Electrons and Size Selection. *Chem. Phys. Lett.* 2013, *579*, 1−10.

(9) Zurek, E.; Edwards, P. P.; Hoffmann, R. A Molecular Perspective on Lithium-Ammonia Solutions. *Angew. Chem., Int. Ed.* 2009, *48*, 8198−8232.

(10) West, A. H. C.; Yoder, B. L.; Luckhaus, D.; Signorell, R. Solvated Electrons in Clusters: Magic Numbers for the Photoelectron Anisotropy. *J. Phys. Chem. A* 2015, *119*, 12376−12382.

(11) Gunina, A. O.; Krylov, A. I. Probing Electronic Wave Functions of Sodium-Doped Clusters: Dyson Orbitals, Anisotropy Parameters, and Ionization Cross-Sections. *J. Phys. Chem. A* 2016, *120*, 9841−9856.

(12) Borgis, D.; Rossky, P. J.; Turi, L. Electronic Excited State Lifetimes of Anionic Water Clusters: Dependence on Charge Solvation Motif. *J. Phys. Chem. Lett.* 2017, *8*, 2304−2309.

(13) Bartels, C.; Hock, C.; Huwer, J.; Kuhnen, R.; Schwöbel, J.; von Issendorff, B. Probing the Angular Momentum Character of the Valence Orbitals of Free Sodium Nanoclusters. *Science* 2009, *323*, 1323−1327.

(14) Bartels, C. Angular Distributions of Photoelectrons from Cold, Size-Selected Sodium Cluster Anions. *Ph.D. Dissertation*, Albert-Ludwigs-Universität, Freiburg im Breisgau, Germany, 2008.

(15) Rolles, D.; Zhang, H.; Pešić, Z. D.; Bilodeau, R. C.; Wills, A.; Kukk, E.; Rude, B. S.; Ackerman, G. D.; Bozek, J. D.; Díez Muiño, R.; et al. Size Effects in Angle-Resolved Photoelectron Spectroscopy of Free Rare-Gas Clusters. *Phys. Rev. A: At., Mol., Opt. Phys.* 2007, *75*, 031201.

(16) Sanov, A. Laboratory-Frame Photoelectron Angular Distributions in Anion Photodetachment: Insight into Electronic Structure and Intermolecular Interactions. *Annu. Rev. Phys. Chem.* 2014, *65*, 341−363.

(17) Melko, J. J.; Castleman, A. W., Jr. Photoelectron Imaging of Small Aluminum Clusters: Quantifying s-p Hybridization. *Phys. Chem. Chem. Phys.* 2013, *15*, 3173−3178.

(18) Khuseynov, D.; Blackstone, C. C.; Culberson, L. M.; Sanov, A. Photoelectron Angular Distributions for States of Any Mixed Character: An Experiment-Friendly Model for Atomic, Molecular, and Cluster Anions. *J. Chem. Phys.* 2014, *141*, 124312.

(19) Kammrath, A.; Verlet, J. R. R.; Griffin, G. B.; Neumark, D. M. Photoelectron Imaging of Large Anionic Methanol Clusters: $(MeOH)_n^-$ (n ∼ 70−460). *J. Chem. Phys.* 2006, *125*, 171102.

(20) Young, R. M.; Yandell, M. A.; Niemeyer, M.; Neumark, D. M. Photoelectron Imaging of Tetrahydrofuran Cluster Anions $(THF)_n^-$ (1 ≤ n ≤ 100). *J. Chem. Phys.* 2010, *133*, 154312.

(21) Signorell, R.; Yoder, B. L.; West, A. H. C.; Ferreiro, J. J.; Saak, C.-M. Angle-Resolved Valence Shell Photoelectron Spectroscopy of Neutral Nanosized Molecular Aggregates. *Chem. Sci.* 2014, *5*, 1283−1295.

(22) West, A. H. C.; Yoder, B. L.; Signorell, R. Size-Dependent Velocity Map Photoelectron Imaging of Nanosized Ammonia Aerosol Particles. *J. Phys. Chem. A* 2013, *117*, 13326−13335.

(23) Yoder, B. L.; West, A. H. C.; Schläppi, B.; Chasovskikh, E.; Signorell, R. A Velocity Map Imaging Photoelectron Spectrometer for the Study of Ultrafine Aerosols with a Table-Top VUV Laser and Na-Doping for Particle Sizing Applied to Dimethyl Ether Condensation. *J. Chem. Phys.* 2013, *138*, 044202.

(24) West, A. H. C.; Yoder, B. L.; Luckhaus, D.; Saak, C.-M.; Doppelbauer, M.; Signorell, R. Angle-Resolved Photoemission of Solvated Electrons in Sodium-Doped Clusters. *J. Phys. Chem. Lett.* 2015, *6*, 1487−1492.

(25) Oana, C. M.; Krylov, A. I. Dyson Orbitals for Ionization from the Ground and Electronically Excited States within Equation-of-Motion Coupled-Cluster Formalism: Theory, Implementation, and Examples. *J. Chem. Phys.* 2007, *127*, 234106.

(26) Oana, C. M.; Krylov, A. I. Cross Sections and Photoelectron Angular Distributions in Photodetachment from Negative Ions Using Equation-of-Motion Coupled-Cluster Dyson Orbitals. *J. Chem. Phys.* 2009, *131*, 124114.

(27) Yamamoto, Y.-I.; Suzuki, Y.-I.; Tomasello, G.; Horio, T.; Karashima, S.; Mitrić, R.; Suzuki, T. Time- and Angle-Resolved Photoemission Spectroscopy of Hydrated Electrons near a Liquid Water Surface. *Phys. Rev. Lett.* 2014, *112*, 187603.

(28) Peppernick, S. J.; Gunaratne, K. D. D.; Castleman, A. W., Jr. Superatom Spectroscopy and the Electronic State Correlation between Elements and Isoelectronic Molecular Counterparts. *Proc. Natl. Acad. Sci. U. S. A.* 2010, *107*, 975−980.

(29) Humeniuk, A.; Wohlgemuth, M.; Suzuki, T.; Mitrić, R. Time-Resolved Photoelectron Imaging Spectra from Non-Adiabatic Molecular Dynamics Simulations. *J. Chem. Phys.* 2013, *139*, 134104.

(30) Hopkins, W. S.; Woodham, A. P.; Tonge, N. M.; Ellis, A. M.; Mackenzie, S. R. Photodissociation Dynamics of $Li(NH_3)_4$.: A Velocity Map Imaging Study. *J. Phys. Chem. Lett.* 2011, *2*, 257−261.

(31) Varriale, L.; Tonge, N. M.; Bhalla, N.; Ellis, A. M. Communications: The Electronic Spectrum of $Li(NH_3)_4$. *J. Chem. Phys.* 2010, *132*, 161101.

(32) Salter, T. E.; Ellis, A. M. Microsolvation of Lithium in Ammonia: Dissociation Energies and Spectroscopic Parameters of Small $Li(NH_3)_n$ Clusters (n = 1 and 2) and Their Cations. *Chem. Phys.* 2007, *332*, 132−138.

(33) Salter, T. E.; Mikhailov, V. A.; Evans, C. J.; Ellis, A. M. Infrared Spectroscopy of $Li(NH_3)_n$ Clusters for n = 4−7. *J. Chem. Phys.* 2006, *125*, 034302.

(34) More, M. B.; Glendening, E. D.; Ray, D.; Feller, D.; Armentrout, P. B. Cation-Ether Complexes in the Gas Phase: Bond Dissociation Energies and Equilibrium Structures of $Li^+[O(CH_3)_2]_x$, x = 1−4. *J. Phys. Chem.* 1996, *100*, 1605−1614.

(35) Sohnlein, B. R.; Li, S. G.; Fuller, J. F.; Yang, D. S. Pulsed-Field Ionization Electron Spectroscopy and Binding Energies of Alkali Metal Dimethyl Ether and -Dimethoxyethane Complexes. *J. Chem. Phys.* 2005, *123*, 014318.

(36) Takasu, R.; Hashimoto, K.; Fuke, K. Study on Microscopic Solvation Process of Li Atom in Ammonia Clusters: Photoionization and Photoelectron Spectroscopies of $M(NH_3)_n$ (M = Li, Li^-). *Chem. Phys. Lett.* 1996, *258*, 94−100.

(37) Yoder, B. L.; Litman, J. H.; Forysinski, P. W.; Corbett, J. L.; Signorell, R. Sizer for Neutral Weakly Bound Ultrafine Aerosol Particles Based on Sodium Doping and Mass Spectrometric Detection. *J. Phys. Chem. Lett.* 2011, *2*, 2623−2628.

(38) Litman, J. H.; Yoder, B. L.; Schläppi, B.; Signorell, R. Sodium-Doping as a Reference to Study the Influence of Intracluster Chemistry on the Fragmentation of Weakly-Bound Clusters Upon Vacuum Ultraviolet Photoionization. *Phys. Chem. Chem. Phys.* 2013, *15*, 940−949.

(39) Forysinski, P. W.; Zielke, P.; Luckhaus, D.; Corbett, J.; Signorell, R. Photoionization of Small Sodium-Doped Acetic Acid Clusters. *J. Chem. Phys.* 2011, *134*, 094314.

(40) Chandler, D. W.; Houston, P. L. Two-Dimensional Imaging of State-Selected Photodissociation Products Detected by Multiphoton Ionization. *J. Chem. Phys.* 1987, *87*, 1445−1447.

(41) Eppink, A.; Parker, D. H. Velocity Map Imaging of Ions and Electrons Using Electrostatic Lenses: Application in Photoelectron and Photofragment Ion Imaging of Molecular Oxygen. *Rev. Sci. Instrum.* 1997, *68*, 3477−3484.

(42) Dick, B. Inverting Ion Images without Abel Inversion: Maximum Entropy Reconstruction of Velocity Maps. *Phys. Chem. Chem. Phys.* 2014, *16*, 570−580.

(43) Garcia, G. A.; Nahon, L.; Powis, I. Two-Dimensional Charged Particle Image Inversion Using a Polar Basis Function Expansion. *Rev. Sci. Instrum.* 2004, *75*, 4989−4996.

(44) Cooper, J.; Zare, R. N. Angular Distribution of Photoelectrons. *J. Chem. Phys.* 1968, *48*, 942−943.

(45) Frisch, M. J.; Trucks, G. W.; Schlegel, H. B.; Scuseria, G. E.; Robb, M. A.; Cheeseman, J. R.; Scalmani, G.; Barone, V.; Mennucci, B.; Petersson, G. A.; et al. *Gaussian 09*; Gaussian, Inc.: Wallingford, CT, USA, 2009.

(46) Reed, A. E.; Weinstock, R. B.; Weinhold, F. Natural-Population Analysis. *J. Chem. Phys.* **1985**, *83*, 735−746.

(47) Acree, W. E.; Chickos, J. S. Phase Transition Enthalpy Measurements of Organic and Organometallic Compounds. In *Nist Chemistry Webbook, Nist Standard Reference Database Number 69*; Linstrom, P. J., Mallard, W. G., Eds.; National Institute of Standards and Technology: Gaithersburg, MD; retrieved December 18, 2018.

(48) Peterson, K. I.; Dao, P. D.; Farley, R. W.; Castleman, A. W. Photoionization of Sodium Clusters. *J. Chem. Phys.* **1984**, *80*, 1780−1785.

(49) Bushaw, B. A.; Nörtershauser, W.; Drake, G. W. F.; Kluge, H. J. Ionization Energy of ^{6,7}Li Determined by Triple-Resonance Laser Spectroscopy. *Phys. Rev. A: At., Mol., Opt. Phys.* **2007**, *75*, 052503.

(50) Holton, D.; Edwards, P. Metals in Non-Aqueous Solvents. *Chem. Britain* **1985**, *21*, 1007−1013.

(51) Thomas, J. M.; Edwards, P. P.; Kuznetsov, V. L. Sir Humphry Davy: Boundless Chemist, Physicist, Poet and Man of Action. *ChemPhysChem* **2008**, *9*, 59−66.

(52) Seel, A. G.; Swan, H.; Bowron, D. T.; Wasse, J. C.; Weller, T.; Edwards, P. P.; Howard, C. A.; Skipper, N. T. Electron Solvation and the Unique Liquid Structure of a Mixed-Amine Expanded Metal: The Saturated Li-NH3-MeNH$_2$ System. *Angew. Chem., Int. Ed.* **2017**, *56*, 1561−1565.

(53) Hartweg, S.; West, A. H. C.; Yoder, B. L.; Signorell, R. Metal Transition in Sodium-Ammonia Nanodroplets. *Angew. Chem., Int. Ed.* **2016**, *55*, 12347−12350.

(54) Coons, M. P.; You, Z. Q.; Herbert, J. M. The Hydrated Electron at the Surface of Neat Liquid Water Appears to Be Indistinguishable from the Bulk Species. *J. Am. Chem. Soc.* **2016**, *138*, 10879−10886.

(55) Karashima, S.; Yamamoto, Y.; Suzuki, T. Resolving Non-adiabatic Dynamics of Hydrated Electrons Using Ultrafast Photo-emission Anisotropy. *Phys. Rev. Lett.* **2016**, *116*, 137601.

(56) Luckhaus, D.; Yamamoto, Y. I.; Suzuki, T.; Signorell, R. Genuine Binding Energy of the Hydrated Electron. *Sci. Adv.* **2017**, *3*, e1603224.

(57) Elkins, M. H.; Williams, H. L.; Shreve, A. T.; Neumark, D. M. Relaxation Mechanism of the Hydrated Electron. *Science* **2013**, *342*, 1496−1499.

(58) Stähler, J.; Deinert, J. C.; Wegkamp, D.; Hagen, S.; Wolf, M. Real-Time Measurement of the Vertical Binding Energy During the Birth of a Solvated Electron. *J. Am. Chem. Soc.* **2015**, *137*, 3520−3524.

(59) Riley, J. W.; Wang, B. X.; Woodhouse, J. L.; Assmann, M.; Worth, G. A.; Fielding, H. H. Unravelling the Role of an Aqueous Environment on the Electronic Structure and Ionization of Phenol Using Photoelectron Spectroscopy. *J. Phys. Chem. Lett.* **2018**, *9*, 678−682.

(60) Savolainen, J.; Uhlig, F.; Ahmed, S.; Hamm, P.; Jungwirth, P. Direct Observation of the Collapse of the Delocalized Excess Electron in Water. *Nat. Chem.* **2014**, *6*, 697−701.

(61) Kumar, G.; Roy, A.; McMullen, R. S.; Kutagulla, S.; Bradforth, S. E. The Influence of Aqueous Solvent on the Electronic Structure and Non-Adiabatic Dynamics of Indole Explored by Liquid-Jet Photoelectron Spectroscopy. *Faraday Discuss.* **2018**, *212*, 359−381.